iScience

CellPress
OPEN ACCESS

Article

CircTBC1D22A inhibits the progression of colorectal cancer through autophagy regulated via miR-1825/ATG14 axis

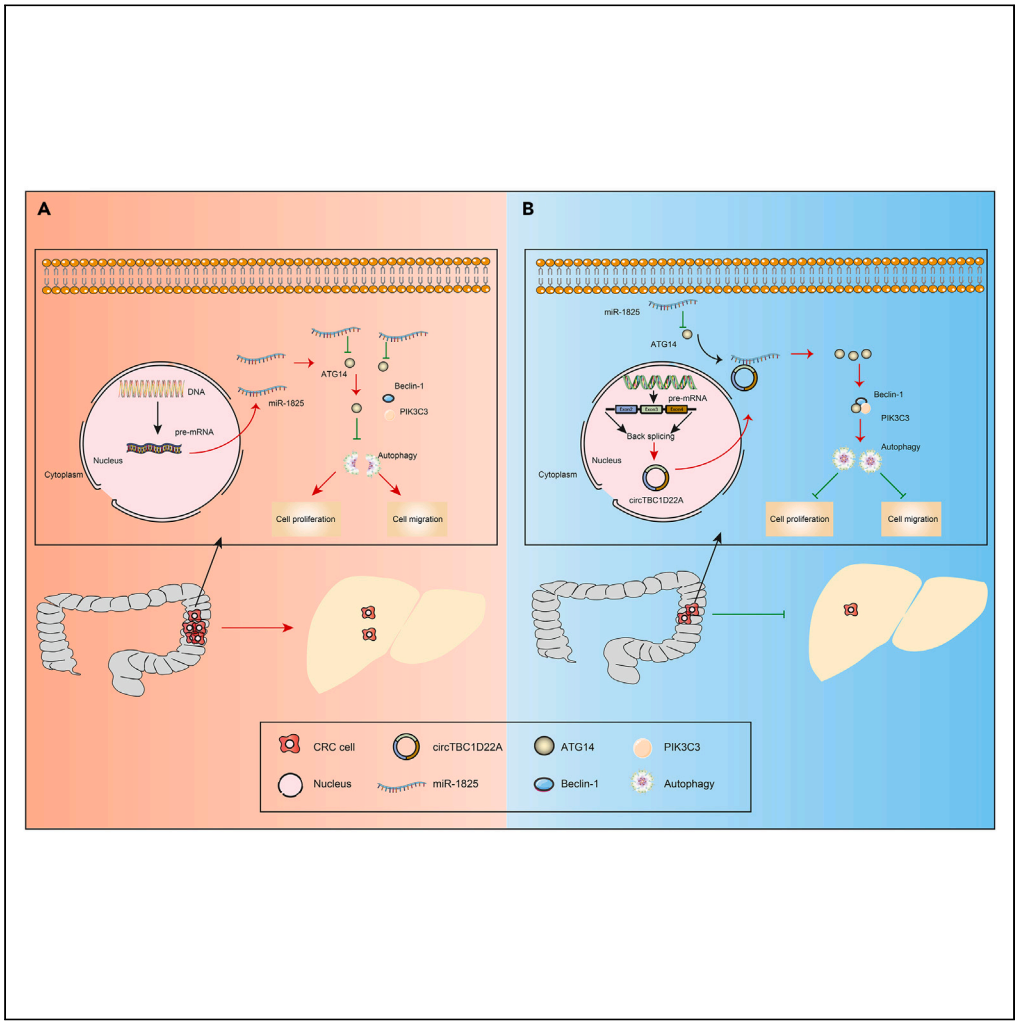

Jingbo Sun, Hongmei Wu, Junjie Luo, ..., Lixin Liu, Xiaolong Liu, Qingling Zhang

llx0129@i.smu.edu.cn (L.L.)
lxl1979@i.smu.edu.cn (X.L.)
zqllc8@126.com (Q.Z.)

Highlights

miR-1825 is upregulated in CRC and associated with CRC progression

circTBC1D22A functions as an efficient miR-1825 sponge in CRC cells

ATG14 is functional target of miR-1825 in CRC cells

circTBC1D22A regulates autophagy via miR-1825/ATG14 axis

Sun et al., iScience 27, 109168
March 15, 2024 © 2024
https://doi.org/10.1016/j.isci.2024.109168

iScience

CellPress
OPEN ACCESS

Article

CircTBC1D22A inhibits the progression of colorectal cancer through autophagy regulated via miR-1825/ATG14 axis

Jingbo Sun,[1,2,3,4] Hongmei Wu,[1,2,4] Junjie Luo,[3,4] Yue Qiu,[1,2,4] Yanyan Li,[1,2] Yangwei Xu,[2] Lixin Liu,[3,*] Xiaolong Liu,[3,*] and Qingling Zhang[1,2,5,*]

SUMMARY

Distant metastasis is the main cause of death in patients with colorectal cancer (CRC). A better understanding of the mechanisms of metastasis can greatly improve the outcome of patients with CRC. Accumulating evidence suggests that circRNA plays pivotal roles in cancer progression and metastasis, especially acting as a miRNA sponge to regulate the expression of the target gene. A public database bioinformatics analysis found that miR-1825 was highly expressed in CRC tissues. In this study, miR-1825 was highly expressed in CRC tissues, which was positively correlated with lymph node metastasis and distant metastasis. *In vitro* and *in vivo* experiments confirmed that miR-1825 was positively correlated with the proliferation and migration of CRC cells. This event can be inhibited by circTBC1D22A. CircTBC1D22A can directly interact with miR-1825 and subsequently act as a miRNA sponge to regulate the expression of the target gene ATG14, which collectively advances the autophagy-mediated progression and metastasis of CRC.

INTRODUCTION

Colorectal cancer (CRC) is a highly prevalent malignancy worldwide, ranking third and fifth in cancer incidence and mortality in China, respectively. Despite an increased awareness of the pathogenic risk of CRC and advances in treatment strategies, there has been no substantial breakthrough in the clinical treatment of tumor metastasis, and liver metastasis is one of the major causes of death in CRC.[1,2] Therefore, it is urgent to identify therapeutic targets by further exploring the underlying mechanisms of CRC metastasis.

Non-coding RNAs (ncRNAs) consist of microRNAs (miRNAs), long non-coding RNAs (lncRNAs), and circular RNAs (circRNAs), which play crucial roles in tumor progression.[3] Most of the circRNAs are a large class of primarily ncRNAs that mainly derive from the back-splicing of pre-mRNA transcripts and are characterized as covalently closed loop structures.[4] circRNAs have key roles in cancer development and progression through diverse mechanisms.[5] The tissue-restricted and cancer-specific expression characteristics make circRNAs have strong potential as diagnostic, prognostic, and predictive biomarkers.[6,7] And circRNAs function as competitive endogenous RNAs (ceRNAs) to sponge miRNAs and inhibit their function.[8,9] miRNAs regulate gene expression by directly interacting with the 3′ untranslated region (UTR) of target mRNAs and play a central role in the ceRNA hypothesis.[10] However, the interactions and functions of circRNAs and miRNAs in CRC metastasis have not been fully discussed; Thus, it is of great value to analyze specific circRNAs and elucidate their functions and mechanisms in mediating CRC progression.

Autophagy was defined in mammalian cells as an intracellular degradation system that delivers cytoplasmic materials to lysosomes. Autophagy is an essential mechanism for maintaining cellular integrity and genomic stability, and deletion of autophagy-related (ATG) proteins can affect this homeostasis and thus may initiate cellular tumor development.[11] Disruption of autophagy can drive dormant breast cancer stem cell activation into metastatic tumors.[12] The autophagy of breast cancer cells restricts local and metastatic recurrence after primary tumor excision.[13] DDX5 promoted autophagy and reduced liver cancer cell proliferation and tumorigenesis by binding to p62 and interfering with the p62/TRAF6 interaction.[14] ATG14 (Autophagy Related 14, ATG14) interacts directly with Beclin-1 in the class III phosphatidylinositol 3-kinase complex, causing an increase in the number and size of autophagic vesicles and thus activating autophagy. Moreover, the binding of ATG14 and Beclin-1 is necessary for autophagosome formation.[15,16] Accumulating evidence has revealed that ATG14 promotes chemoresistance in pancreatic cancer,[17] ovarian cancer,[18] and CRC[19] through activating autophagy. However, there is no complete and systematic study on the correlation between the circRNA-miRNA-ATG14 axis and tumor metastasis in CRC.

[1]Department of Pathology, School of Basic Medical Sciences, Southern Medical University, Guangzhou, Guangdong 510515, People's Republic of China
[2]Department of Pathology, Guangdong Provincial People's Hospital (Guangdong Academy of Medical Sciences), Southern Medical University, Guangzhou 510080, Guangdong Province, People's Republic of China
[3]Department of General Surgery, The Third Affiliated Hospital of Southern Medical University, 183 West Zhongshan Avenue, Guangzhou 510630, Guangdong, People's Republic of China
[4]These authors contributed equally
[5]Lead contact
*Correspondence: llx0129@i.smu.edu.cn (L.L.), lxl1979@i.smu.edu.cn (X.L.), zqllc8@126.com (Q.Z.)
https://doi.org/10.1016/j.isci.2024.109168

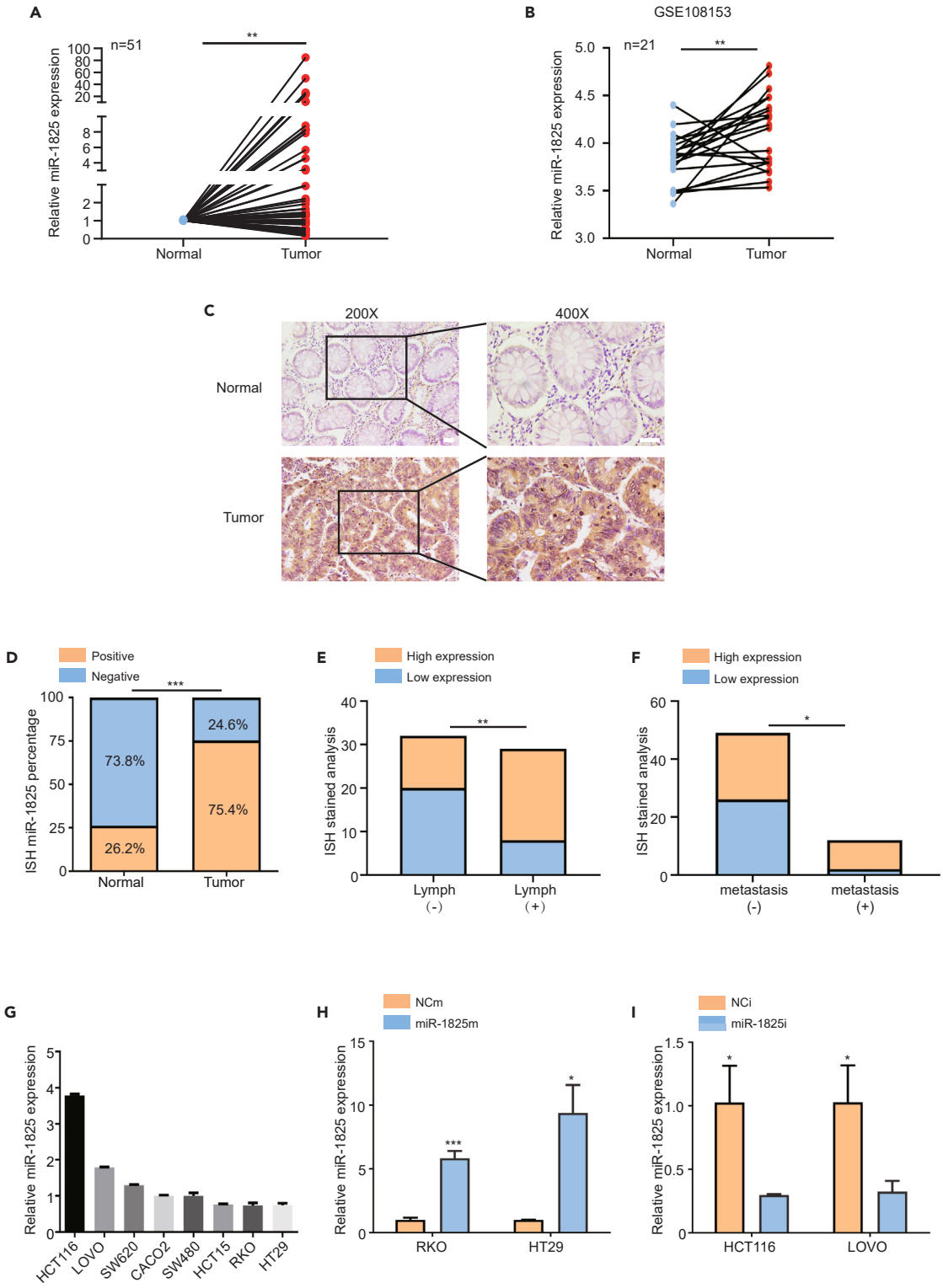

Figure 1. miR-1825 is upregulated in CRC and associated with CRC progression

(A) Relative RNA level of miR-1825 in 51 CRC tissues and paired adjacent normal tissues, as determined by RT-PCR. Relative expression levels were normalized to U6. **p < 0.01, paired t-test.

(B) Relative RNA level of miR-1825 in CRC tissues and paired adjacent normal tissues in GSE108153 dataset, **p < 0.01, two-tailed Student's *t* test.

(C) Representative micrographs images of miR-1825 ISH staining in normal colorectal mucosa and CRC tissues. Scale bars, 20 μm.

Figure 1. *Continued*

(D) Percentage of miR-1825 ISH in CRC and matched adjacent normal colorectal mucosa tissues. n = 61. ***p < 0.001, Chi-square test.

(E) ISH staining analysis of miR-1825 expression in CRC tissues with or without lymph node metastasis. n = 61. **p < 0.01, Chi-square test.

(F) ISH staining analysis of miR-1825 expression in CRC tissues with or without distant metastasis. n = 61. *p < 0.05, Chi-square test.

(G) RT-PCR analyzes the basic expression of miR-1825 in CRC cell lines.

(H and I) RT-PCR analyzes the relative expression of miR-1825 in indicated cell lines. *p < 0.05, ***p < 0.001, means ± SD, two-tailed Student's *t* test.

In this study, based on bioinformatics analysis and a series of *in vitro* and *in vivo* experiments, we first determined that miR-1825 was positively correlated with the proliferation and migration of CRC cells, while the upstream regulator circTBC1D22A showed the opposite effect. Further mechanistic investigations indicated that circTBC1D22A functioned as a sponge of miR-1825 to upregulate ATG14, thereby mediating autophagy and inhibiting the proliferation and migration of CRC. These results deepen our understanding of CRC progression and may provide feasible therapeutic strategies for patients with CRC.

RESULTS

miR-1825 is upregulated in colorectal cancer and associated with colorectal cancer progression

Previous work has found that miR-1825 and miR-1246 are upregulated in both tissue and serum samples of CRC.[20] The role of miR-1246 in CRC and the related molecular mechanisms have been relatively well studied, including its effects on the proliferation and metastatic capacity of CRC cells and its role in the metastatic microenvironment.[21–23] However, the biological function of miR-1825 in CRC and its molecular mechanisms related to the progression of CRC are still unknown. To investigate the role and molecular mechanism of miR-1825 in CRC, we analyzed the expression of miR-1825 in CRC tissues. RT-PCR results confirmed that miR-1825 expression was higher in 51 CRC tissues than that in the paired colorectal mucosa ($p < 0.01$, Figure 1A). Consistently, we also found that miR-1825 was significantly more highly expressed in CRC compared with normal colorectal tissues in the GEO (GSE108153) database (Figure 1B). We performed ISH staining of miR-1825 using 61 cases of CRC tissue samples (Figure 1C) and the level of miR-1825 expression was significantly higher in CRC than in paired colorectal mucosa (Figure 1D). In addition, statistical analysis of clinical characteristics showed that high miR-1825 expression was highly correlated with lymph node metastasis and distant metastasis in patients with CRC (Figures 1E and 1F; Table 1). There is a tendency for the expression level of miR-1825 to be higher in T4 tumors than in T1-3 tumors, but the difference was not big enough to reach statistical significance (Table 1). Taken together, these results suggest that miR-1825 may play a crucial role in promoting CRC progression and metastasis.

miR-1825 promotes colorectal cancer proliferation and migration

To further investigate the function of miR-1825 in CRC progression, the endogenous expression of miR-1825 was analyzed in eight CRC cell lines (HCT116, LOVO, SW620, CACO2, SW480, HCT15, RKO, and HT29) (Figure 1G). Two stable miR-1825 overexpressing cell lines RKO (RKO.miR-1825m), HT29 (HT29.miR-1825m) (Figure 1H), and two miR-1825 knockdown cell lines HCT116 (HCT116.miR-1825i) and LOVO

Table 1. Clinical characteristics of patients with CRC with low miR-1825 expression and high miR-1825 expression

		miR-1825 expression		
	Cases	Low	High	p value
Age (years)				
<60	36	15	21	p = 0.4257
≥60	25	13	12	
Gender				
Male	42	21	21	p = 0.3396
Female	19	7	12	
T stage				
T1–T3	25	15	10	p = 0.0656
T4	36	13	23	
Lymph node metastasis				
–	32	20	12	p = 0.0063
+	29	8	21	
Distant metastasis				
–	49	26	23	p = 0.0234
+	12	2	10	

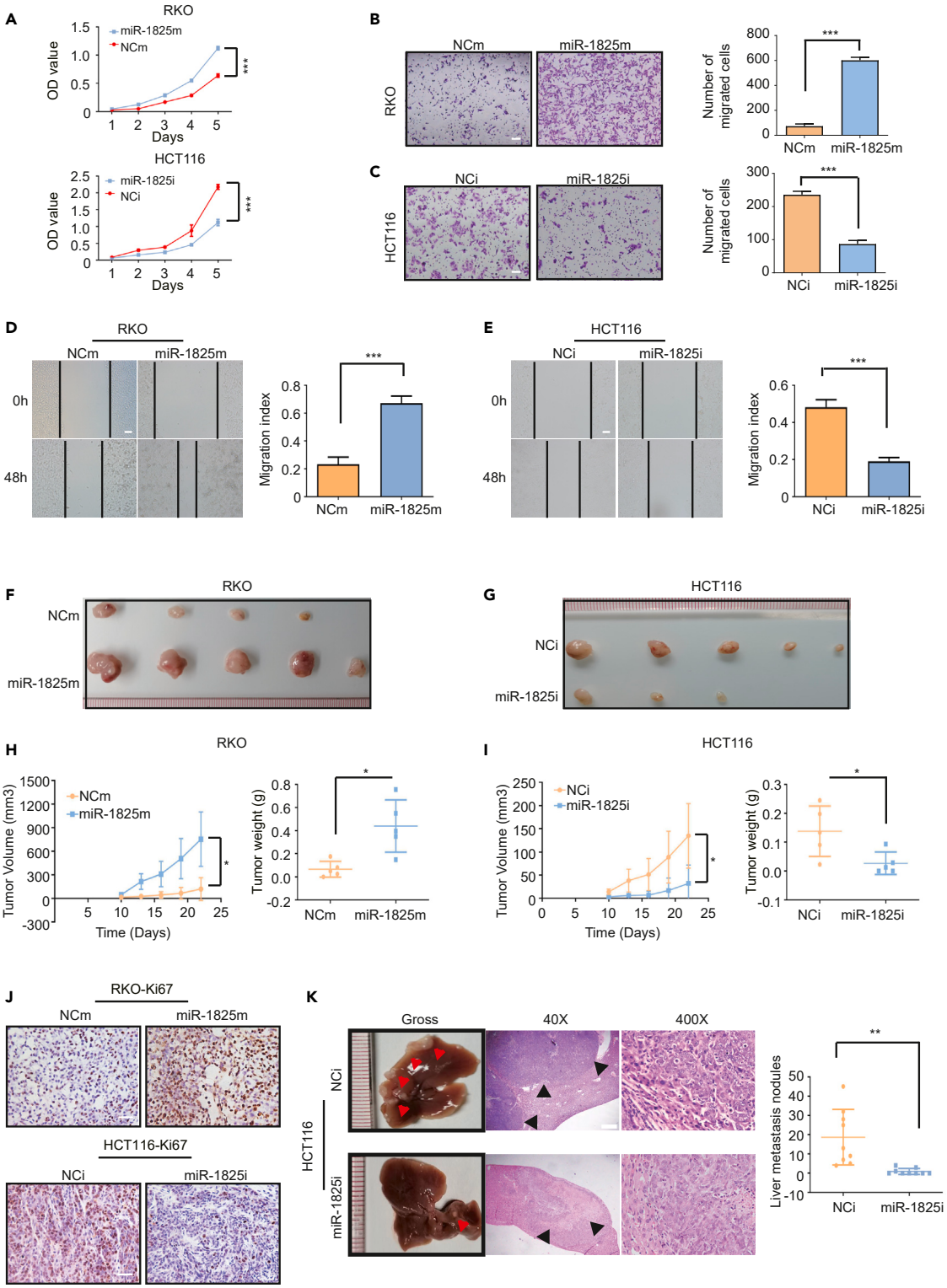

Figure 2. miR-1825 promotes CRC proliferation and migration *in vitro* and *in vivo*

(A) CCK8 assay analysis of the indicated cell lines.

(B and C) Transwell analyzes the migration of the indicated cell lines. Scale bars, 100 μm.

(D and E) Wound healing assay analyzes the migration of the indicated cell lines. Scale bars, 100 μm.

(F and G) Images of gross CRC subcutaneous xenograft tumor models formed by the indicated cell lines.

Figure 2. *Continued*

(H and I) Tumor volume and weight analyses for the CRC subcutaneous xenograft tumor. Means ± SD are provided (n = 5).

(J) The percentage of positively stained Ki-67 cells in subcutaneous xenograft tumor models. Scale bars, 20 μm.

(K) Gross and H&E staining observe the liver metastasis in indicated cell lines. Each arrow pointed a liver metastasis nodule. Means ± SD are provided (n = 9). The scale bar at 40× magnification represents 200 μm. The scale bar at 400× magnification represents 20 μm. *p < 0.05, **p < 0.01, ***p < 0.001, means ± SD, two-tailed Student's *t* test.

(LOVO.miR-1825i) (Figure 1I) were established for the following experiments. The CCK8 assay results showed that the proliferation abilities were significantly increased compared with control cells (RKO.NCm and HT29.NCm) after miR-1825 overexpression (RKO.miR-1825m and HT29.miR-1825m), while these abilities were significantly inhibited in HCT116.miR-1825i and LOVO.miR-1825i cells (Figures 2A, S1A, and S1B). Transwell and wound healing assay results showed that the migration abilities of the miR-1825 overexpression cells were significantly enhanced compared to control cells. In contrast, these abilities were inhibited in the miR-1825 knockdown cells (Figures 2B–2E and S1C–S1F). These results suggest that miR-1825 significantly promotes the proliferation and migration abilities of CRC cells.

To further investigate the functions of miR-1825 *in vivo*, subcutaneous xenograft tumor models were established to assess the effect of miR-1825 on tumor growth. It revealed that miR-1825 can positively regulate CRC tumor growth (Figures 2F–2I). The Ki-67 index was higher in the RKO.miR-1825m group and lower in the HCT116.miR-1825i group than that observed in the controls (Figures 2J, S1G, and S1H). In addition, the hepatic metastasis model observation showed fewer liver metastatic nodules occurred in the HCT116.miR-1825i group (Figure 2K). Taken together, these results demonstrate that miR-1825 could dramatically promote CRC growth and metastasis.

circTBC1D22A functions as an efficient miR-1825 sponge in colorectal cancer

Current studies have revealed that circRNAs most often function as ceRNAs to regulate downstream mRNAs by sponging miRNAs. To identify potential ceRNAs for miR-1825 in CRC, circRNA-seq was performed using six CRC tissues that were divided into high miR-1825 expression and low miR-1825 expression. Of these, 100 circRNAs were elevated, and 78 circRNAs were reduced (Figures 3A–3C). We selected the 78 down-regulated circRNAs in CRC for further analysis and then selected 28 circRNAs that potential sponge miR-1825 predicted by targetscan, RNAhybrid, or circinteractome (Figure S2A). What is more, among the circRNAs detected, circTBC1D22A appeared to be the most significant miRNA pulled down by the miR-1825 probe (Figure 3D). To confirm this prediction, the predicted miR-1825 binding site in the 3′ UTR of circTBC1D22A (wild type) or the mutated sequence (mutant type) were cloned into luciferase reporter plasmids (Figure S2B) and assessed for their response to miR-1825. Notably, the luciferase activity of the 3′UTR of circTBC1D22A was suppressed by miR-1825 in the circTBC1D22A-WT group, whereas it had no change in the circTBC1D22A-MUT group (Figure 3E). In addition, resistance to digestion with RNase R treatment confirmed that this RNA species is circular (Figure 3F). These results suggest that circTBC1D22A is directly bound to and sponged miR-1825, and might participate in the function of miR-1825 in CRC.

CircTBC1D22A (hsa_circ_0001251), a novel circRNA, is located in chromosome 22 and consists of exons 2–4 (575 bp) from the TBC1D22A gene as reported in circBase (Figure S3A). However, the role of circTBC1D22A in CRC has not been reported. To explore the biological functions of circTBC1D22A, we transfected lentivirus vectors expressing circTBC1D22A and siRNAs of circTBC1D22A into CRC cells (Figures S3B and S3C). The CCK8 assay results showed that the proliferation abilities were significantly decreased compared with control cells after circTBC1D22A overexpression, while these abilities were significantly increased after silencing circTBC1D22A (Figures 3G, S4A, and S4B). Transwell and wound healing assay results showed that the migration abilities of the circTBC1D22A overexpression cells were significantly inhibited compared to control cells. In contrast, these abilities were enhanced in the silencing circTBC1D22A cells (Figures 3H, 3I, and S4C–S4F). These results suggest that circTBC1D22A could suppress the proliferation and migration abilities of CRC cells.

Moreover, rescue experiments were performed by co-transfecting miR-1825 and circTBC1D22A overexpression vectors in RKO. Remarkably, we found that miR-1825 promoted the proliferation and migration of CRC cells, which could be rescued by the overexpression of circTBC1D22A (Figures 3J–3L). Taken together, these results demonstrate that circTBC1D22A could affect the proliferation and migration abilities of CRC cells via miR-1825.

ATG14 is a functional target of miR-1825 in colorectal cancer cells

To explore how miR-1825 could regulate CRC progression, three mRNAtarget-predicting algorithms (Targetscan, miRWalk, and miRDIP) were utilized to identify the potential downstream targets of miR-1825 (Figure S5A). Among these candidates, ATG14 was overlapped among all databases, and ATG14-mediated regulation of autophagy has been reported to be involved in tumor progression. Furthermore, we introduced the mCherry-EGFP-LC3B reporter to determine the role of miR-1825 in autophagic flux. The green and red dots represent phagosomes and autolysosomes, respectively, and the yellow dots represent autophagosomes. The autophagic activity indicated by the formation of autophagosomes is determined by quantifying the yellow dots. Overexpression of miR-1825 reduced the number of red spots, and conversely, knockdown of miR-1825 increased the number of red spots (Figures 4A and 4B). To confirm this prediction, the predicted miR-1825 binding site in the 3′ UTR of ATG14 (wild type) or the mutated sequence (mutant type) were cloned into luciferase reporter plasmids (Figure S5B) and assessed for their response to miR-1825 in RKO. Notably, the luciferase activity of the 3′UTR of ATG14 was suppressed by miR-1825 in the ATG14-WT group, whereas it had no change in the ATG14-MUT group (Figure 4C). Moreover, ectopic expression of miR-1825 in CRC cells suppressed the expression of ATG14. Conversely, knocking down of miR-1825 resulted in the upregulation of ATG14 (Figures 4D and S5C). Previous studies have demonstrated that ATG14 is a key regulatory protein associated with cellular autophagy

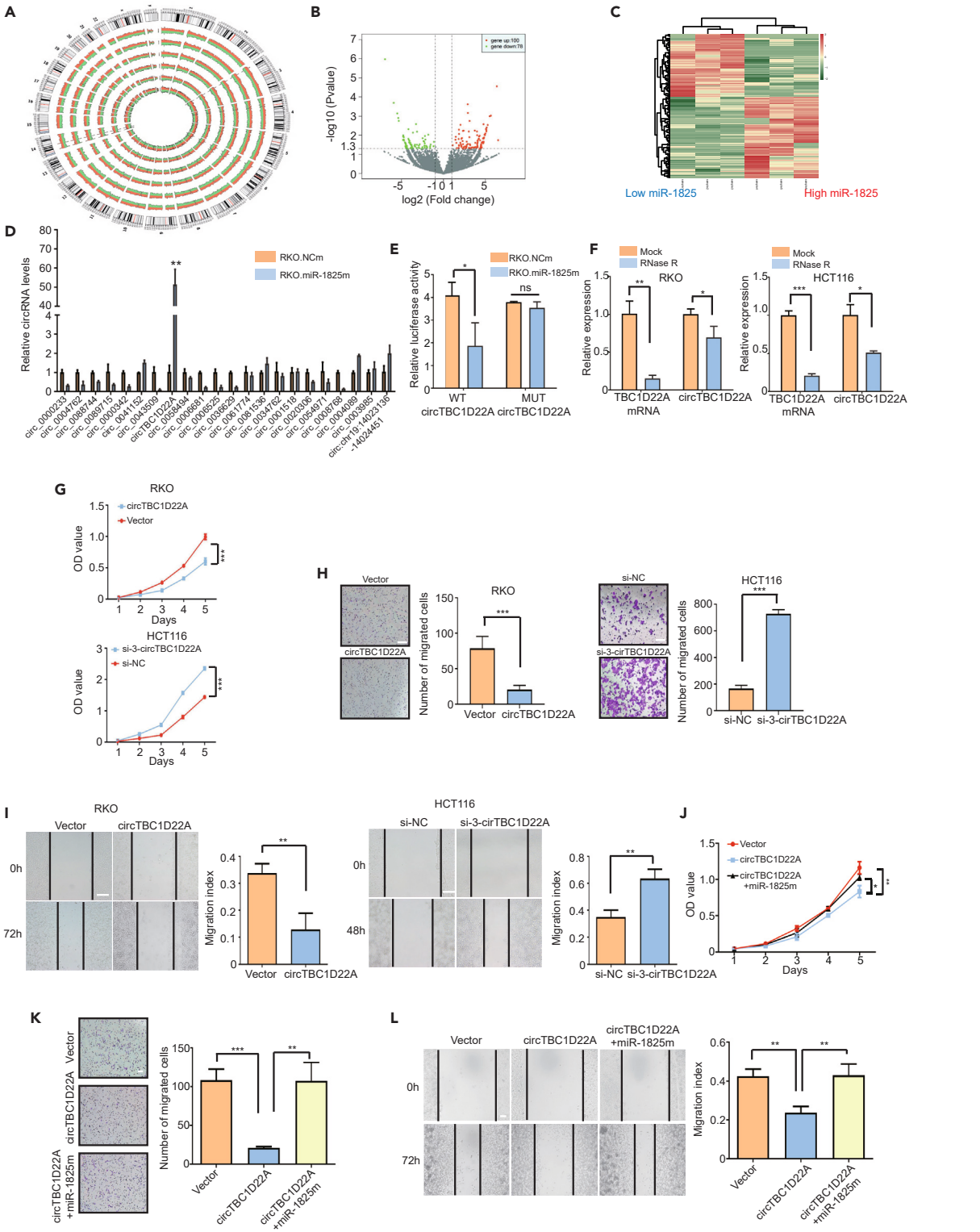

Figure 3. circTBC1D22A functions as an efficient miR-1825 sponge in CRC

(A) Differentially expressed RNAs of circRNAs expression profile analysis in circos.

(B) The volcano map of circRNA differential expression profiles between three miR-1825 low expression samples and three miR-1825 high expression samples.

(C) A heatmap of deferentially expressed circRNAs.

Figure 3. *Continued*

(D) Fold-enrichment of 22 circRNAs that were pulled down by biotin-miR-1825 in RKO cell line and circTBC1D22A was the most enriched ceRNA.

(E) Luciferase activities of 3′UTR circTBC1D22A-luc constructs in RKO cell line after the overexpression of miR-1825. Means ± SD are provided (n = 3). *p < 0.05, means ± SD, two-tailed Student's *t* test.

(F) The abundance of circTBC1D22A and linear TBC1D22A mRNA in CRC cells treated with RNase R was determined by RT-PCR (normalized to mock treatment). *p < 0.05, **p < 0.01, ***p < 0.001, means ± SD, two-tailed Student's *t* test.

(G) CCK8 assay analysis of the indicated cell lines.

(H) Transwell analyzes the migration of the indicated cell lines. Scale bars, 100 μm.

(I) Wound healing assay analyzes the migration of the indicated cell lines. Scale bars, 100 μm.

(J) Effects of circTBC1D22A and miR-1825/circTBC1D22A on the proliferation ability of RKO cell line by CCK8 assay.

(K and L) Effects of circTBC1D22A and miR-1825/circTBC1D22A on the migration ability of RKO cell line by transwell assay and wound healing. Scale bars, 100 μm *p < 0.05, **p < 0.01, ***p < 0.001, means ± SD, two-tailed Student's *t* test.

and that ATG14 upregulates the expression of PIK3C3 and Beclin-1 to mediate autophagy.[24,25] Overexpression of miR-1825 in RKO and HT29 decreased the levels of ATG14, PIK3C3, Beclin-1, and LC3-II, while knockdown of miR-1825 increased those in HCT116 and LOVO (Figure 4E). In addition, we explored whether Beclin-1 and PIK3C3 are downstream targets of miR-1825. Based on bioinformatics analysis, the miTG scores of ATG14, Beclin-1, and PIK3C3 in DIANA TOOLS were 0.935, 0.752, and none. In addition, the total context++ scores of ATG14, Beclin-1, and PIK3C3 in TargetScan were −0.29, −0.15, and none (Figure S5D). The predicted miR-1825 binding site in the 3′ UTR of Beclin-1 (wild type) or the mutated sequence (mutant type) were cloned into luciferase reporter plasmids and assessed for their response to miR-1825 in RKO. However, the luciferase activity of the 3′ UTR of Beclin-1 did not change in the Beclin-1-WT and MUT groups (Figure S5E). These results indicate that miR-1825 could suppress autophagy by directly binding to the 3′ UTR region of ATG14, but not Beclin-1 and PIK3C3.

ATG14 rescues the oncogenic function of miR-1825

In the GEPIA dataset and GSE8671 cohort, we found that ATG14 was significantly lower in CRC than in normal tissues (Figures S6A–S6C). To further investigate the function of ATG14 in CRC progression, we selected the most efficient siRNA of ATG14 to experiment with (Figure S6D). Meanwhile, we detected the efficiency of ATG14 overexpression (Figure S6E). The CCK8 assay results showed that the proliferation abilities were significantly inhibited after ATG14 overexpression in HCT116, while these abilities were significantly increased in RKO.si2-ATG14 cells (Figure S6F). Transwell assay results showed that the migration abilities of the ATG14 overexpression cells were significantly inhibited compared to control cells. In contrast, these abilities were enhanced in RKO.si2-ATG14 cells (Figure S6G). These results suggest that ATG14 might act as a tumor suppressor in CRC. Rescue experiments were conducted to investigate whether miR-1825 promoted CRC progression by mediating autophagy. The western blot and autophagic flux assay results showed that the overexpression of ATG14 abolished the inhibitory effect of miR-1825 on autophagy (Figures 5A–5C). Furthermore, the CCK8 assay, transwell assay, and wound healing assay results showed that ATG14 dramatically reversed the promoting effects of miR-1825 on the proliferation and migration of CRC cells (Figures 5D–5I). Additionally, we analyzed the expression relations of miR-1825 with ATG14 *in vivo*. ISH and IHC staining results demonstrated that miR-1825 could inhibit the expression of ATG14, Beclin-1, and LC3 (Figure 5J). Collectively, these results demonstrate that miR-1825 promotes CRC progression via suppressing ATG14 expression.

CircTBC1D22A-miR-1825-ATG14 axis regulated autophagy

To investigate the relationship of circTBC1D22A with miR-1825 and ATG14, RT-PCR was performed and confirmed our hypothesis that circTBC1D22A could effectively inhibit miR-1825 to restore ATG14 expression (Figures 6A and 6B). Overexpression of circTBC1D22A in RKO and HT29 increased the levels of ATG14, PIK3C3, Beclin-1, and LC3-II, while silencing circTBC1D22A decreased that in HCT116 and LOVO (Figure 6C). The western blot and autophagic flux assay results further revealed that the overexpression of circTBC1D22A abolished the inhibitory effect of miR-1825 on autophagy in the rescue experiments, indicating that circTBC1D22A could regulate autophagy via miR-1825/ATG14 (Figures 6D–6F). Furthermore, we also detected the expression of the circTBC1D22A-miR-1825-ATG14 axis. In the cohort of 51 samples, RNA extracted from 6 samples failed to generate enough materials for detection. RT-PCR results confirmed that the expression of ATG14 and circTBC1D22A was lower in 45 CRC tissues than in the paired colorectal mucosa (Figures 6G and 6H). There was a negative correlation between miR-1825 and circTBC1D22A and ATG14, while there was a positive correlation between circTBC1D22A and ATG14 in 45 CRC samples (Figures 6I–6K). Also, the AKT-mTOR pathway is known to inhibit autophagy.[26] And we found that miR-1825 could activate the AKT-mTOR pathway in CRC cell lines, while circTBC1D22A could inhibit the activation of the AKT-mTOR pathway (Figures S7A and S7B). The block experiments were conducted to investigate the relationship between tumor biology and the circTBC1D22A/miR-1825/ATG14 axis. The CCK8 assay and Transwell assay results showed that the autophagy inhibitor chloroquine (CQ) significantly reversed the inhibitory effects of circTBC1D22A on the proliferation and migration of CRC cells (Figures S8A and S8B). Therefore, these results further confirm the vital role of the circTBC1D22A-miR-1825 axis in autophagy-mediated CRC progression.

DISCUSSION

Recently, increasing evidence has shown that ncRNAs participate in regulating malignant phenotypes and act as critical clinical biomarkers for diagnosis and prognosis in diverse cancers.[3,27] Recently, miR-1825 has been reported to be aberrantly expressed in different tumors such as

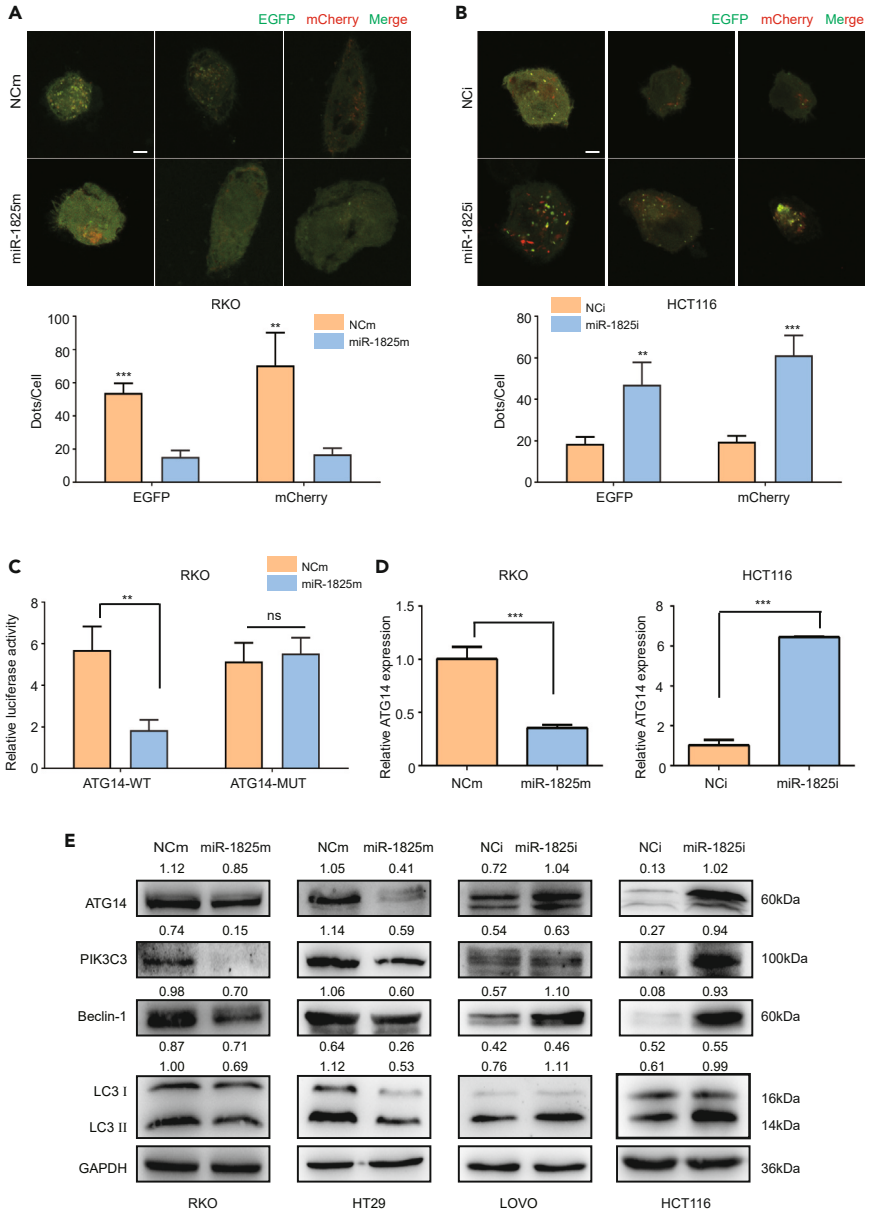

Figure 4. ATG14 is functional target of miR-1825 in CRC cells

(A and B) The distributions of mCherry-EGFP-LC3B in RKO and HCT116 cell lines were analyzed by confocal microscopy after overexpression or knockdown of miR-1825 (n = 5) and three representative images are presented. Scale bars, 5 μm.

(C) Luciferase activities of 3′UTR ATG14-luc constructs in RKO cell line after the overexpression of miR-1825. Means ± SD are provided (n = 3). **p < 0.01, means ± SD, two-tailed Student's *t* test.

(D) RT-PCR analyzes the relative expression of ATG14 in RKO and HCT116 cell lines after transfection. ***p < 0.001, means ± SD, two-tailed Student's *t* test.

(E) ATG14, PIK3C3, Beclin-1, and LC3B expression in the indicated cell lines were analyzed by western blot after overexpression or knockdown of miR-1825.

prostate cancer,[28] hepatocellular carcinoma,[29] and CRC.[20] However, the biological function of miR-1825 in CRC has not been reported. In this study, we first identified miR-1825 as a key miRNA involved in CRC progression. miR-1825 was markedly upregulated in CRC specimens, and miR-1825 expression positively correlated with lymph node metastasis and distant metastasis in human patients with CRC. Functional experiments indicated that miR-1825 significantly facilitated the proliferation and migration of CRC cells. Then circRNA-seq was performed to identify potential ceRNAs for miR-1825 in CRC. The results revealed that circTBC1D22A significantly reduced the activity of miR-1825 and suppressed its functions by sponging it. Therefore, a mechanism was proposed that circTBC1D22A functioned as a sponge of miR-1825 to upregulate ATG14, thereby mediating autophagy and inhibiting the proliferation and migration of CRC.

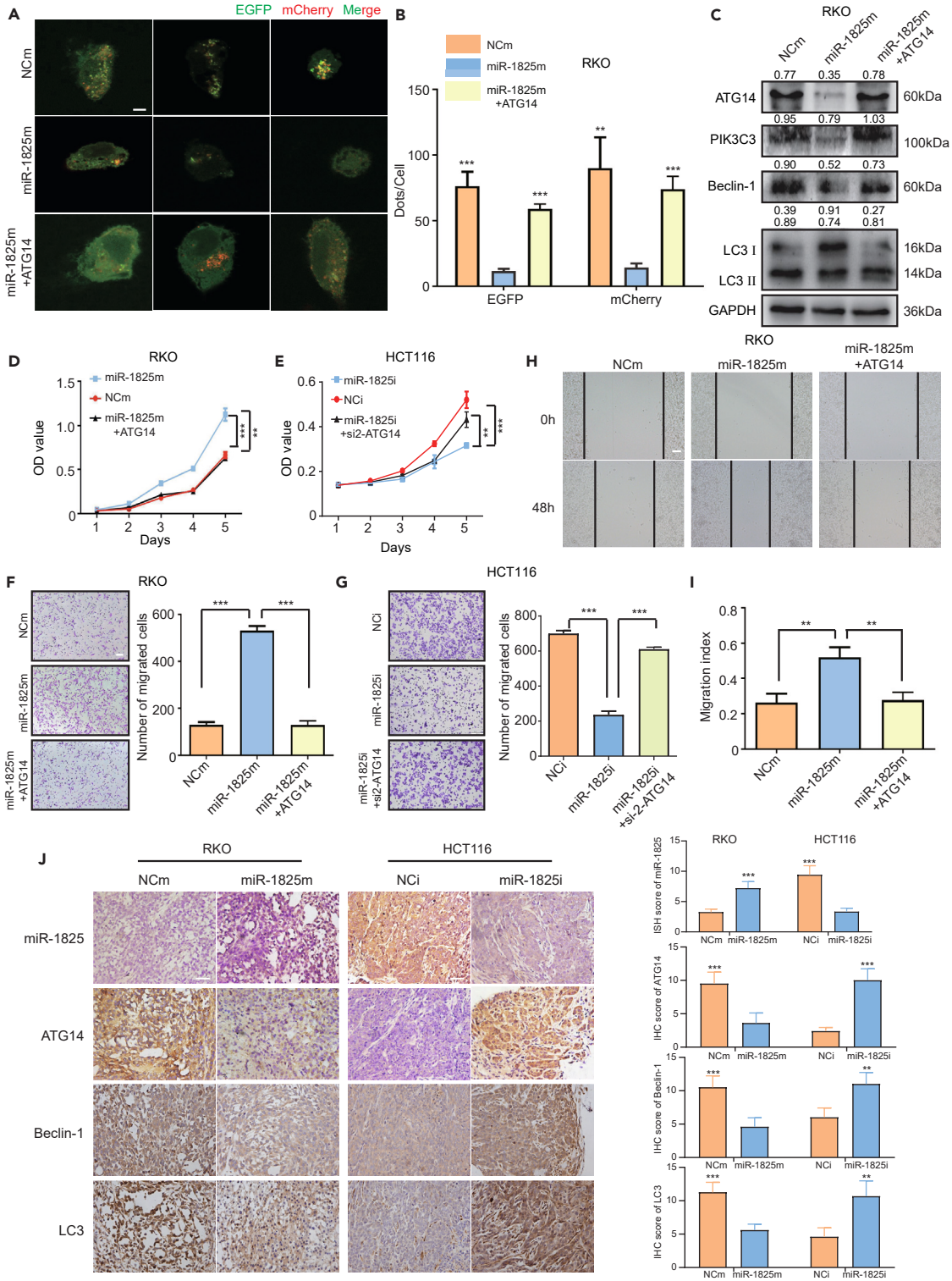

Figure 5. ATG14 rescues the oncogenic function of miR-1825

(A and B) The distributions of mCherry-EGFP-LC3B in miR-1825 overexpressing or miR-1825/ATG14 co-expressing RKO cell lines were analyzed by confocal microscopy (n = 5) and three representative images are presented. Scale bars, 5 μm.

(C) ATG14, PIK3C3, Beclin-1, LC3B expression in miR-1825 overexpressing or miR-1825/ATG14 co-expressing RKO cell lines were analyzed by western blot.

(D) Effects of miR-1825 and miR-1825/ATG14 on the proliferation ability of RKO cell line by CCK8 assay.

Figure 5. *Continued*

(E) Effects of miR-1825i and miR-1825i/si-2-ATG14 on the proliferation ability of HCT116 cell line by CCK8 assay.

(F, H, and I) Effects of miR-1825 and miR-1825/ATG14 on the migration ability of RKO cell line by transwell assay and wound healing.

(G) Effects of miR-1825i and miR-1825i/si-2-ATG14 on the migration ability of HCT116 cell line by transwell assay. Scale bars, 100 μm. $^{**}p < 0.01$, $^{***}p < 0.001$, means ± SD, two-tailed Student's *t* test.

(J) ISH staining of miR-1825 and IHC staining of ATG14, Beclin-1 and LC3 in subcutaneous xenograft tumor models. Scale bars, 20 μm.

Previous studies have found that miR-1825 participates in various pathological conditions such as amyotrophic lateral sclerosis,[30,31] cardiac regeneration,[32] and cancer. Indeed, the function of miR-1825 in tumor progression is still controversial. In glioblastoma, miR-1825 suppressed tumor progression by targeting CDK14 through the Wnt/β-catenin pathway.[33] However, miR-1825 was upregulated and predicted poor prognosis in prostate cancer,[28] hepatocellular carcinoma,[29] and CRC.[20] The molecular mechanism through which miR-1825 regulates CRC metastasis has not been elucidated. In this study, we found that miR-1825 was aberrantly expressed in CRC and enhanced CRC cell proliferation and metastasis. Currently, accumulating evidence indicates that circRNAs are involved in the development and progression of various cancers by sponging specific miRNAs as a ceRNA. For instance, circ_0001666 could suppress the tumorigenesis and metastasis of CRC via sponging miR-576-5p and regulating the expression of PCDH10.[34] Circ_0030167 inhibits invasion, migration, proliferation, and stemness of pancreatic cancer cells via sponging miR-338-5p and targeting the Wif1/Wnt8/β-catenin axis.[35] Unlike common screening circRNA-Seq in which CRC tissues are selected randomly, we selected 3 CRC tissues with high miR-1825 expression and 3 CRC tissues with low miR-1825 expression. Through the circRNA-Seq and bioinformatics analysis, we predicted that multiple circRNA candidates were capable of binding miR-1825. Next, by using the dual-luciferase reporter assay and RNA pull-down assay, the direct binding between miR-1825 and circTBC1D22A was confirmed. It was found that circRNAs can function as "miRNA sponges" and then inhibit their functions. Consistently, rescue experiments confirmed that circTBC1D22A could partially reverse the effect of miR-1825 suggesting that circTBC1D22A acts as a tumor suppressor by inhibiting miR-1825 in CRC.

Autophagy is critical for tumor progression, and ncRNAs have been reported to be involved in cancer-associated autophagy.[36,37] For instance, circST3GAL6 regulates autophagy-mediated tumor progression through the FOXP2/MET/mTOR axis in gastric cancer.[38] CircPARD3 promotes the malignant progression of laryngeal squamous cell carcinoma by inhibiting autophagy.[39] We found that circTBC1D22A could regulate autophagy-mediated proliferation and migration by sponging miR-1825. Cytoplasmic circRNAs usually act as sponges for miRNAs to regulate the expression of downstream target genes. Further studies revealed miR-1825 directly targeted ATG14 to inhibit autophagy in CRC cells. Importantly, we found the involvement of circTBC1D22A in the regulatory role of miR-1825 in ATG14 expression. CircTBC1D22A increased ATG14 expression level via sponging miR-1825, which subsequently activated autophagy and its downstream pathway.

ATG14 (also called Barkor or ATG14L) is considered to be an essential beclin-1-associated autophagy regulator,[16,40] but its role in CRC progression has not been elucidated. Previous studies have revealed that ATG14 promotes chemoresistance in a variety of tumors through activating autophagy.[17–19] ATG14 acts as a direct downstream effector of the SNHG14/miR-186 axis to promote tumor CRC progression.[19] In contrast to previous studies, our results showed that the level of ATG14 expression was significantly lower in CRC than that in normal tissues. Furthermore, ATG14 inhibits the ability of proliferation and migration in CRC cells. These results suggest that ATG14 might act as a tumor suppressor in CRC. Similarly, a recent study has shown that the overexpression of ATG14 inhibited cell viability in HeLa cells.[41] Through our rescue experiment, ATG14 was able to eliminate the miR-1825 upregulation-causing promotion of the proliferation and migration of CRC cells via the activation of autophagy. Consistent with it, our results verified that circTBC1D22A further regulated autophagy through the miR-1825/ATG14 axis in CRC. Finally, we also found a negative correlation between miR-1825 and circTBC1D22A and ATG14, while a positive correlation between circTBC1D22A and ATG14, which was analyzed and confirmed in patients with CRC. However, more work remains to be done for further exploration to validate the effects of ATG14 on circTBC1D22A-mediated autophagy in CRC. Interestingly, we found that miR-1825 could activate the AKT-mTOR pathway in CRC cell lines, while circTBC1D22A could inhibit the activation of the AKT-mTOR pathway. And the AKT-mTOR pathway is known to inhibit autophagy and is a classical signaling pathway that promotes cancer progression.[26]

In summary, this is the first report on the aberrant expression of circTBC1D22A/miR-1825/ATG14 in CRC. More importantly, we found that circTBC1D22A could regulate autophagy-mediated proliferation and migration through the miR-1825/ATG14 pathway. The above results proved that circTBC1D22A/miR-1825/ATG14 axis might become a potential therapeutic target for CRC in the future.

Limitations of the study

There exist various shortcomings and constraints in our present investigation. It is imperative for our forthcoming research to delve deeper into the inquiry of whether miR-1825 governs the mechanisms of autophagy, CRC cell migration, and proliferation, specifically via ATG14 or the AKT-mTOR pathway, or possibly through both pathways.

STAR★METHODS

Detailed methods are provided in the online version of this paper and include the following:

- KEY RESOURCES TABLE
- RESOURCE AVAILABILITY

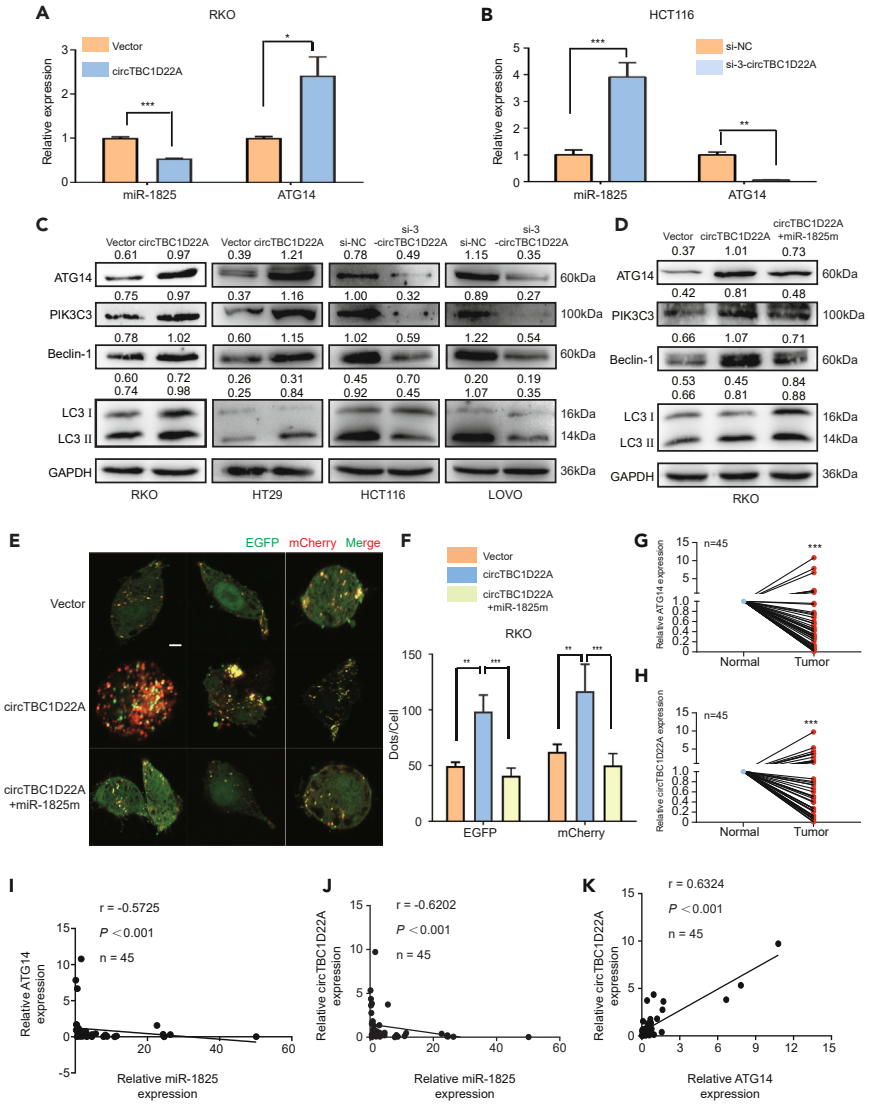

Figure 6. CircTBC1D22A regulates autophagy via miR-1825/ATG14

(A and B) RT-PCR analyzes the relative expression of miR-1825 and ATG14 in RKO and HCT116 cell lines after transfection. *p < 0.05, **p < 0.01, ***p < 0.001, means ± SD, two-tailed Student's *t* test.

(C) ATG14, PIK3C3, Beclin-1, and LC3B expression in the indicated cell lines were analyzed by western blot after overexpression or knockdown of circTBC1D22 A.

(D) ATG14, PIK3C3, Beclin-1, LC3B expression in circTBC1D22A overexpressing or miR-1825/circTBC1D22A co-expressing RKO cell lines were analyzed by western blot.

(E and F) The distributions of mCherry-EGFP-LC3B in circTBC1D22A overexpressing or miR-1825/circTBC1D22A co-expressing RKO cell lines were analyzed by confocal microscopy (n = 5) and three representative images are presented. Scale bars, 5 μm.

(G and H) Relative RNA level of ATG14 and circTBC1D22A in 45 CRC tissues and paired adjacent normal tissues, as determined by RT-PCR. Relative expression levels were normalized to GAPDH. ***p < 0.001, paired t-test.

(I–K) Pearson correlation analysis was conducted to analyze the relation between circTBC1D22A, miR-1825 and ATG14 in 45 CRC tissues. *p < 0.05, **p < 0.01, ***p < 0.001.

- ○ Lead contact
- ○ Materials availability
- ○ Data and code availability

- ● EXPERIMENTAL MODEL AND STUDY PARTICIPANT DETAILS
  - ○ Clinical samples
  - ○ Cell culture
  - ○ Animal experiments

SUPPLEMENTAL INFORMATION

Supplemental information can be found online at https://doi.org/10.1016/j.isci.2024.109168.

ACKNOWLEDGMENTS

The authors would like to thank Dr Zhicheng Zeng (Department of Pathology, School of Basic Medical Sciences, Southern Medical University, Guangzhou, Guangdong 510515, People's Republic of China) for providing technical support. This project was supported by grants of the National Natural Science Foundation of China (Q.L.Z, 81772918, 8197227 and 82173033; Y.W.X, 82102712); China Postdoctoral Science Foundation (Y.W.X, 2021M690751); Key Area Research and Development Program of Guangdong Province (Q.L.Z, 2021B0101420005); High-level Hospital Construction Project (Q.L.Z, DFJHBF202108); Guangdong Basic and Applied Basic Research Foundation (X.L.L, 2022A1515012290) and President Foundation of The Third Affiliated Hospital of Southern Medical University (X.L.L, YM202208, YP202217 and J.B.S, YQ202214).

AUTHOR CONTRIBUTIONS

J.B.S, H.M.W, J.J.L, and Y.Q carried out the experiments. J.B.S, H.M.W, J.J.L, and Y.Q contributed equally to this work. Y.Q, Y.Y.L, and Y.W.X participated in data analysis and animal experiments. L.X.L and X.L.L gave assisted in collecting tissue samples. Q.L.Z and J.B.S designed the study and wrote the article. All authors read and approved the final article.

DECLARATION OF INTERESTS

The authors declare no competing interests.

Received: September 1, 2023
Revised: November 23, 2023
Accepted: February 6, 2024
Published: February 12, 2024

REFERENCES

1. Brenner, H., Kloor, M., and Pox, C.P. (2014). Colorectal cancer. Lancet *383*, 1490–1502. https://doi.org/10.1016/S0140-6736(13)61649-9.
2. Zheng, R., Zeng, H., Zhang, S., Chen, T., and Chen, W. (2016). National estimates of cancer prevalence in China, 2011. Cancer Lett. *370*, 33–38. https://doi.org/10.1016/j.canlet.2015.10.003.
3. Chen, L., He, M., Zhang, M., Sun, Q., Zeng, S., Zhao, H., Yang, H., Liu, M., Ren, S., Meng, X., and Xu, H. (2021). The Role of non-coding RNAs in colorectal cancer, with a focus on its autophagy. Pharmacol. Ther. *226*, 107868. https://doi.org/10.1016/j.pharmthera.2021.107868.
4. Misir, S., Wu, N., and Yang, B.B. (2022). Specific expression and functions of circular RNAs. Cell Death Differ. *29*, 481–491. https://doi.org/10.1038/s41418-022-00948-7.
5. Kristensen, L.S., Jakobsen, T., Hager, H., and Kjems, J. (2022). The emerging roles of circRNAs in cancer and oncology. Nat. Rev. Clin. Oncol. *19*, 188–206. https://doi.org/10.1038/s41571-021-00585-y.
6. He, A.T., Liu, J., Li, F., and Yang, B.B. (2021). Targeting circular RNAs as a therapeutic approach: current strategies and challenges. Signal Transduct. Target. Ther. *6*, 185. https://doi.org/10.1038/s41392-021-00569-5.
7. Wang, H., Meng, Q., Qian, J., Li, M., Gu, C., and Yang, Y. (2022). Review: RNA-based diagnostic markers discovery and therapeutic targets development in cancer. Pharmacol. Ther. *234*, 108123. https://doi.org/10.1016/j.pharmthera.2022.108123.
8. Long, F., Lin, Z., Li, L., Ma, M., Lu, Z., Jing, L., Li, X., and Lin, C. (2021). Comprehensive landscape and future perspectives of circular RNAs in colorectal cancer. Mol. Cancer *20*, 26. https://doi.org/10.1186/s12943-021-01318-6.
9. Li, J., Sun, D., Pu, W., Wang, J., and Peng, Y. (2020). Circular RNAs in Cancer: Biogenesis, Function, and Clinical Significance. Trends Cancer *6*, 319–336. https://doi.org/10.1016/j.trecan.2020.01.012.
10. Dragomir, M.P., Knutsen, E., and Calin, G.A. (2022). Classical and noncanonical functions of miRNAs in cancers. Trends Genet. *38*, 379–394. https://doi.org/10.1016/j.tig.2021.10.002.
11. Morishita, H., and Mizushima, N. (2019). Diverse Cellular Roles of Autophagy. Annu. Rev. Cell Dev. Biol. *35*, 453–475. https://doi.org/10.1146/annurev-cellbio-100818-125300.
12. La Belle Flynn, A., Calhoun, B.C., Sharma, A., Chang, J.C., Almasan, A., and Schiemann, W.P. (2019). Autophagy inhibition elicits emergence from metastatic dormancy by inducing and stabilizing Pfkfb3 expression. Nat. Commun. *10*, 3668. https://doi.org/10.1038/s41467-019-11640-9.
13. Marsh, T., Kenific, C.M., Suresh, D., Gonzalez, H., Shamir, E.R., Mei, W., Tankka, A., Leidal, A.M., Kalavacherla, S., Woo, K., et al. (2020). Autophagic Degradation of NBR1 Restricts Metastatic Outgrowth during Mammary Tumor Progression. Dev. Cell *52*, 591–604.e6. https://doi.org/10.1016/j.devcel.2020.01.025.
14. Zhang, H., Zhang, Y., Zhu, X., Chen, C., Zhang, C., Xia, Y., Zhao, Y., Andrisani, O., and Kong, L. (2019). DEAD Box Protein 5 Inhibits Liver Tumorigenesis by Stimulating Autophagy via Interaction with p62/SQSTM1.

Hepatology *69*, 1046–1063. https://doi.org/10.1002/hep.30300.

15. Menon, M.B., and Dhamija, S. (2018). Beclin 1 Phosphorylation - at the Center of Autophagy Regulation. Front. Cell Dev. Biol. *6*, 137. https://doi.org/10.3389/fcell.2018.00137.
16. Sun, Q., Fan, W., Chen, K., Ding, X., Chen, S., and Zhong, Q. (2008). Identification of Barkor as a mammalian autophagy-specific factor for Beclin 1 and class III phosphatidylinositol 3-kinase. Proc. Natl. Acad. Sci. USA *105*, 19211–19216. https://doi.org/10.1073/pnas.0810452105.
17. Zhou, C., Yi, C., Yi, Y., Qin, W., Yan, Y., Dong, X., Zhang, X., Huang, Y., Zhang, R., Wei, J., et al. (2020). LncRNA PVT1 promotes gemcitabine resistance of pancreatic cancer via activating Wnt/beta-catenin and autophagy pathway through modulating the miR-619-5p/Pygo2 and miR-619-5p/ATG14 axes. Mol. Cancer *19*, 118. https://doi.org/10.1186/s12943-020-01237-y.
18. Hu, Z., Cai, M., Zhang, Y., Tao, L., and Guo, R. (2020). miR-29c-3p inhibits autophagy and cisplatin resistance in ovarian cancer by regulating FOXP1/ATG14 pathway. Cell Cycle *19*, 193–206. https://doi.org/10.1080/15384101.2019.1704537.
19. Han, Y., Zhou, S., Wang, X., Mao, E., and Huang, L. (2020). SNHG14 stimulates cell autophagy to facilitate cisplatin resistance of colorectal cancer by regulating miR-186/ATG14 axis. Biomed. Pharmacother. *121*, 109580. https://doi.org/10.1016/j.biopha.2019.109580.
20. Pruseth, B., Ghosh, A., Pradhan, D., Purkait, S., and Guttula, P.K. (2021). Analysis of Overexpressed miRNA in Circulation and Cancer Tissue to Develop a Potential microRNA Panel for the Diagnosis of Colorectal Cancer. MicroRNA *10*, 250–262. https://doi.org/10.2174/2211536611666211228102644.
21. Cooks, T., Pateras, I.S., Jenkins, L.M., Patel, K.M., Robles, A.I., Morris, J., Forshew, T., Appella, E., Gorgoulis, V.G., and Harris, C.C. (2018). Mutant p53 cancers reprogram macrophages to tumor supporting macrophages via exosomal miR-1246. Nat. Commun. *9*, 771. https://doi.org/10.1038/s41467-018-03224-w.
22. Guo, S., Chen, J., Chen, F., Zeng, Q., Liu, W.L., and Zhang, G. (2020). Exosomes derived from Fusobacterium nucleatum-infected colorectal cancer cells facilitate tumour metastasis by selectively carrying miR-1246/92b-3p/27a-3p and CXCL16. Gut *70*, 1507–1519. https://doi.org/10.1136/gutjnl-2020-321187.
23. Lukosevicius, R., Juzenas, S., Salteniene, V., Kulokiene, U., Arstikyte, J., Hemmrich-Stanisak, G., Franke, A., Link, A., Ruzgys, P., Satkauskas, S., et al. (2022). miRNome Profiling and Functional Analysis Reveal Involvement of hsa-miR-1246 in Colon Adenoma-Carcinoma Transition by Targeting AXIN2 and CFTR. Int. J. Mol. Sci. *23*, 2107. https://doi.org/10.3390/ijms23042107.
24. King, K.E., Losier, T.T., and Russell, R.C. (2021). Regulation of Autophagy Enzymes by Nutrient Signaling. Trends Biochem. Sci. *46*, 687–700. https://doi.org/10.1016/j.tibs.2021.01.006.
25. Fogel, A.I., Dlouhy, B.J., Wang, C., Ryu, S.W., Neutzner, A., Hasson, S.A., Sideris, D.P., Abeliovich, H., and Youle, R.J. (2013). Role of membrane association and Atg14-dependent phosphorylation in beclin-1-mediated autophagy. Mol. Cell Biol. *33*, 3675–3688. https://doi.org/10.1128/MCB.00079-13.
26. Xi, S., Cai, H., Lu, J., Zhang, Y., Yu, Y., Chen, F., Huang, Q., Wang, F., and Chen, Z. (2021). The pseudogene PRELID1P6 promotes glioma progression via the hnHNPH1-Akt/mTOR axis. Oncogene *40*, 4453–4467. https://doi.org/10.1038/s41388-021-01854-x.
27. Liang, J., Zhang, L., and Cheng, W. (2021). Non-coding RNA-mediated autophagy in cancer: A protumor or antitumor factor? Biochim. Biophys. Acta. Rev. Cancer *1876*, 188642. https://doi.org/10.1016/j.bbcan.2021.188642.
28. Guo, X., Han, T., Hu, P., Guo, X., Zhu, C., Wang, Y., and Chang, S. (2018). Five microRNAs in serum as potential biomarkers for prostate cancer risk assessment and therapeutic intervention. Int. Urol. Nephrol. *50*, 2193–2200. https://doi.org/10.1007/s11255-018-2009-4.
29. Pascut, D., Krmac, H., Gilardi, F., Patti, R., Calligaris, R., Crocè, L.S., and Tiribelli, C. (2019). A comparative characterization of the circulating miRNome in whole blood and serum of HCC patients. Sci. Rep. *9*, 8265. https://doi.org/10.1038/s41598-019-44580-x.
30. Helferich, A.M., Brockmann, S.J., Reinders, J., Deshpande, D., Holzmann, K., Brenner, D., Andersen, P.M., Petri, S., Thal, D.R., Michaelis, J., et al. (2018). Dysregulation of a novel miR-1825/TBCB/TUBA4A pathway in sporadic and familial ALS. Cell. Mol. Life Sci. *75*, 4301–4319. https://doi.org/10.1007/s00018-018-2873-1.
31. Aksu-Menges, E., Balci-Hayta, B., Bekircan-Kurt, C.E., Aydinoglu, A.T., Erdem-Ozdamar, S., and Tan, E. (2022). Two distinct skeletal muscle microRNA signatures revealing the complex mechanism of sporadic ALS. Acta Neurol. Belg. *122*, 1499–1509. https://doi.org/10.1007/s13760-021-01743-w.
32. Pandey, R., Velasquez, S., Durrani, S., Jiang, M., Neiman, M., Crocker, J.S., Benoit, J.B., Rubinstein, J., Paul, A., and Ahmed, R.P. (2017). MicroRNA-1825 induces proliferation of adult cardiomyocytes and promotes cardiac regeneration post ischemic injury. Am. J. Transl. Res. *9*, 3120–3137.
33. Lu, F., Li, C., Sun, Y., Jia, T., Li, N., and Li, H. (2020). Upregulation of miR-1825 inhibits the progression of glioblastoma by suppressing CDK14 though Wnt/beta-catenin signaling pathway. World J. Surg. Oncol. *18*, 147. https://doi.org/10.1186/s12957-020-01927-3.
34. Zhou, J., Wang, L., Sun, Q., Chen, R., Zhang, C., Yang, P., Tan, Y., Peng, C., Wang, T., Jin, C., et al. (2021). Hsa_circ_0001666 suppresses the progression of colorectal cancer through the miR-576-5p/PCDH10 axis. Clin. Transl. Med. *11*, e565. https://doi.org/10.1002/ctm2.565.
35. Yao, X., Mao, Y., Wu, D., Zhu, Y., Lu, J., Huang, Y., Guo, Y., Wang, Z., Zhu, S., Li, X., and Lu, Y. (2021). Exosomal circ_0030167 derived from BM-MSCs inhibits the invasion, migration, proliferation and stemness of pancreatic cancer cells by sponging miR-338-5p and targeting the Wif1/Wnt8/beta-catenin axis. Cancer Lett. *512*, 38–50. https://doi.org/10.1016/j.canlet.2021.04.030.
36. Galluzzi, L., Pietrocola, F., Bravo-San Pedro, J.M., Amaravadi, R.K., Baehrecke, E.H., Cecconi, F., Codogno, P., Debnath, J., Gewirtz, D.A., Karantza, V., et al. (2015). Autophagy in malignant transformation and cancer progression. EMBO J. *34*, 856–880. https://doi.org/10.15252/embj.201490784.
37. Matarrese, P., Mattia, G., Pagano, M.T., Pontecorvi, G., Ortona, E., Malorni, W., and Carè, A. (2021). The Sex-Related Interplay between TME and Cancer: On the Critical Role of Estrogen, MicroRNAs and Autophagy. Cancers *13*, 3287. https://doi.org/10.3390/cancers13133287.
38. Xu, P., Zhang, X., Cao, J., Yang, J., Chen, Z., Wang, W., Wang, S., Zhang, L., Xie, L., Fang, L., et al. (2022). The novel role of circular RNA ST3GAL6 on blocking gastric cancer malignant behaviours through autophagy regulated by the FOXP2/MET/mTOR axis. Clin. Transl. Med. *12*, e707. https://doi.org/10.1002/ctm2.707.
39. Gao, W., Guo, H., Niu, M., Zheng, X., Zhang, Y., Xue, X., Bo, Y., Guan, X., Li, Z., Guo, Y., et al. (2020). circPARD3 drives malignant progression and chemoresistance of laryngeal squamous cell carcinoma by inhibiting autophagy through the PRKCI-Akt-mTOR pathway. Mol. Cancer *19*, 166. https://doi.org/10.1186/s12943-020-01279-2.
40. Ohashi, Y. (2021). Activation Mechanisms of the VPS34 Complexes. Cells *10*. https://doi.org/10.3390/cells10113124.
41. Mukhopadhyay, S., Schlaepfer, I.R., Bergman, B.C., Panda, P.K., Praharaj, P.P., Naik, P.P., Agarwal, R., and Bhutia, S.K. (2017). ATG14 facilitated lipophagy in cancer cells induce ER stress mediated mitoptosis through a ROS dependent pathway. Free Radic. Biol. Med. *104*, 199–213. https://doi.org/10.1016/j.freeradbiomed.2017.01.007.
42. Wang, R., Zhang, S., Chen, X., Li, N., Li, J., Jia, R., Pan, Y., and Liang, H. (2018). CircNT5E Acts as a Sponge of miR-422a to Promote Glioblastoma Tumorigenesis. Cancer Res. *78*, 4812–4825. https://doi.org/10.1158/0008-5472.CAN-18-0532.
43. Orom, U.A., and Lund, A.H. (2007). Isolation of microRNA targets using biotinylated synthetic microRNAs. Methods *43*, 162–165. https://doi.org/10.1016/j.ymeth.2007.04.007.

STAR★METHODS

KEY RESOURCES TABLE

REAGENT or RESOURCE	SOURCE	IDENTIFIER
Antibodies		
ATG14	ABclonal	Cat#A7526; RRID: AB_2768053
Ki67	ZSGB Bio	Cat#TA500265; RRID: AB_2266274
Beclin-1	Cell Signaling Technology	Cat#D40C5; RRID: AB_1903911
LC3B	ABclonal	Cat#A19665; RRID: AB_2862723
PIK3C3	ABclonal	Cat#A12295; RRID: AB_2861649
Phospho-AKT	Cell Signaling Technology	Cat#4060; RRID: AB_2315049
Phospho-mTOR	Cell Signaling Technology	Cat#5536; RRID: AB_10691552
GAPDH	Proteintech	Cat#10494-1-AP; RRID: AB_2263076
Bacterial and virus strains		
Lentivirus	Genechem (Shanghai, China)	N/A
mCherry-EGFP-labeled LC3B lentivirus (LPP-CS-mcherry-EGFP-LC3B-Lv105-100)	GeneCopoeia Inc	N/A
Biological samples		
Colorectal cancer tissues and normal colorectal tissues	The Third Affiliated Hospital of Southern Medical University	N/A
Chemicals, peptides, and recombinant proteins		
cell counting kit-8	DOJINDO	Cat#CK04
Lipofectamine 2000 Reagent	Invitrogen	Cat#11668
Trizol	Invitrogen	Cat#15596026
Critical commercial assays		
ISH kit	Boster Co	Cat#MK1030
RNase R	GENESEED	Cat#R0301
Streptavidin magnetic beads	Beaver	Cat#22307-1
Luc-pairTM Duo-Luciferase HS assay kit	GeneCopoeia	Cat#FR201-02
Deposited data		
GSE108153	GEO	https://www.ncbi.nlm.nih.gov/geo/
GSE8671	GEO	https://www.ncbi.nlm.nih.gov/geo/
GEPIA dataset	GEPIA	http://gepia2.cancer-pku.cn/#index
GSE252689 (circRNA-seq)	This paper	https://www.ncbi.nlm.nih.gov/geo/query/acc.cgi?acc=GSE252689
Experimental models: Cell lines		
HCT116	ATCC	Cat#CCL-247
LOVO	ATCC	Cat#CCL-229
SW620	ATCC	Cat#CCL-227
CACO2	ATCC	Cat#HTB-37
SW480	ATCC	Cat#CCL-228
HCT15	ATCC	Cat#CCL-225
RKO	ATCC	Cat#CRL-2577
HT29	ATCC	Cat#HTB-38

(*Continued on next page*)

Continued

REAGENT or RESOURCE	SOURCE	IDENTIFIER
Experimental models: Organisms/strains		
BALB/c nude mice (nu/nu)	Guangdong Medical Laboratory Animal Center	N/A
Oligonucleotides		
See Tables S1 and S2 for oligonucleotide information	This paper	N/A
Recombinant DNA		
pEZ-M14 ATG14	GeneCopoeia Inc	N/A
Software and algorithms		
GraphPad Prism	GraphPad Software	https://www.graphpad.com
Image J	National Institutes of Health (NIH)	https://imagej.nih.gov/ij/

RESOURCE AVAILABILITY

Lead contact

Further information and requests for resources and reagents should be directed to and will be fulfilled by the lead contact, Qingling Zhang (zqllc8@126.com).

Materials availability

This study did not generate new unique reagents.

Data and code availability

- The datasets used and/or analyzed during the current study are available within the manuscript and its supplemental information files. Two CRC datasets and circRNA-seq data were downloaded from GEO datasets (GSE8671, GSE108153 and GSE252689).
- The dataset GSE252689 was generated in this study.
- Any additional information required to reanalyze the data reported in this paper is available from the lead contact upon request.

EXPERIMENTAL MODEL AND STUDY PARTICIPANT DETAILS

Clinical samples

61 Paraffin-embedded CRC samples and 51 fresh CRC tissues were collected from patients undergoing surgical treatment without prior radiotherapy and chemotherapy at the Department of General Surgery in the Third Affiliated Hospital of Southern Medical University. The clinical and demographic information of the patient has been provided in Table S3. Both study protocol and informed consent were approved by the Ethical Committee of the Third Affiliated Hospital of Southern Medical University (ID number 2021-038).

Cell culture

The human CRC cell lines HCT116, LOVO, SW620, CACO2, SW480, HCT15, RKO and HT29 were obtained from the American Type Culture Collection (ATCC), generated, in the Department of Pathology, Nanfang Hospital. These cells were cultured in PPMI-1640 medium containing 10% fetal bovine serum (Thermo Scientific, Waltham, MA, United States) and incubated at 37°C under a humidified atmosphere with 5% CO_2. All cell lines were routinely tested for mycoplasma and the results were negative.

Animal experiments

Four-to-six-week-old male BALB/c nude mice (nu/nu) were purchased from Guangdong Medical Laboratory Animal Center (Guangdong, China) and treated according to the Animal Research Reporting of *In vivo* Experiments (ARRIVE) guidelines. All animal studies were approved by the Animal Care and Use Committee of Guangdong Provincial People's Hospital , Southern Medical University (Study approval number: KY2023-204-01). For the subcutaneous tumor model, 2×10^6 CRC cells were suspended in 100 μL of PBS and injected subcutaneously into the left and right inguinal region of each nude mouse. The tumor volumes were measured every 5 days starting 10 days after injection. After 25 days, mice were sacrificed, and the tumors were collected for further analysis and weighed. The tumor volume was calculated using the following formula: tumor volume (mm^3) = ($width^2 \times length$)/2.

For the hepatic metastasis model, mice were anesthetized and exposed the spleen by the laparotomy. 1.5×10^6 CRC cells were suspended in 100 μL of PBS and injected into the distal part of the spleen with an insulin syringe. Four weeks after injection, the mice were

sacrificed, and the livers were collected for pathologic analysis. The livers were sectioned and stained with hematoxylin and eosin (H&E). Metastatic nodules were counted manually using a microscope.

METHOD DETAILS

Cell transfection

miR-1825 mimics and inhibitor lentivirus (LV-1825m-puro and LV-1825i-puro), lentivirus vectors expressing circTBC1D22A, siRNAs of circTBC1D22A and ATG14 were constructed and generated by Genechem (Shanghai, China). The sequences of miR-1825 mimics and inhibitor lentivirus and siRNAs of circTBC1D22A and ATG14 referred to above were listed in Table S2. In the rescue experiments, cells that stably expressed miR-1825 were transfected with the ATG14 expressing plasmids (pEZ-M14-Vector) (GeneCopoeia Inc). Lipofectamine 2000 Reagent (Invitrogen) was then used to transfect ATG14 expressing plasmids, siRNAs of circTBC1D22A and ATG14 according to the manufacturer' s protocol. After being transfected for 48 h, CRC cells were harvested and assessed by RT-PCR analysis. For the stable cell lines, the efficiency of lentiviral infection could be assessed through RT-PCR after puromycin-selected cells for 1-2 weeks.

Cell proliferation, migration, and wound healing assays

Cell proliferation was assessed using the cell counting kit-8 (CCK8) assay. CRC cells (1000 cells per well) were seeded into 96-well plates in triplicate, and 10 μL of CCK8 (DOJINDO, Japan) solution was added into each well, followed by incubation at 37°C for 2 h. Then, the absorbance was measured at 450 nm using a Microplate Autoreader (Bio-Rad, Hercules, CA, USA).

For cell migration assay, cell suspensions (1×10^5 cells) were diluted into 200 μl of serum-free medium and added to the upper transwell chambers (BD Biosciences, CA, USA) and incubated for 48 h. Cells that had migrated through the filter were stained with crystal violet and counted in five fields per insert for further statistical analysis.

For wound healing assays, cells were seeded into 12-well plates and scratched with a pipette tip after 24 h. Images were observed at the indicated times, and wound width at 48-72 h relative to 0 h was evaluated to assess wound healing. Experiments were repeated three times.

Immunohistochemistry (IHC) and *in situ* hybridization (ISH)

Paraffin-embedded sections of CRC and matched adjacent normal tissue samples were dewaxed from xylene, rehydrated in a graded ethanol series to water. Then, sections were immersed in 3% hydrogen peroxide for 10 min and incubated with primary antibodies overnight at 4°C. Subsequently, corresponding secondary antibodies were applied and incubated for 1 h at RT. Targeted molecules were visualized by using DAB and counterstained with hematoxylin. The following primary antibodies were used: ATG14 (1:100 dilution, ABclonal), Ki67 (1:100 dilution, ZSGB Bio), Beclin-1 (1:200 dilution, Cell Signaling Technology) and LC3B (1:50 dilution, ABclonal).

ISH was performed in tissue sections using ISH kit (Boster Co, Wuhan, China) and the miR-1825 detection probe (Kidan Biosciences co, Guangzhou, China) by following the manufacturer's protocol. ISH assay was performed under RNase-free conditions. Briefly, the intensity of staining ranged from 0 to 3 and the percentage of positively stained cells was scored from 0 to 4. The final staining scores (0-12) were calculated by multiplying the intensity of staining and the percentage scores as follows: 0-1 (-), 2-3 (+), 4-8 (+ + +), and 9-12 (+ + + +). The ISH score of <6 was categorized as a low expression group, and an ISH score of ≥6 was categorized as a high expression group. ISH staining and scoring were performed blindly.

RNA preparation, treatment with RNase R, and quantitative reverse transcription PCR (RT-PCR)

Total RNA was extracted from tissues and cells lines by using Trizol (Invitrogen) according to the manufacturer's instructions. The RNA extracted from CRC cells was divided into two groups: one for RNase R (Geneseed, Guangzhou, China) treatment and the other for control. The treated group was incubated with 3 U/μg of RNase R for 10 min at 37°C. For analysis, RT-PCR was used to detect the expression of TBC1D22A and circTBC1D22A. RT-PCR was conducted using SYBR Green PCR Master Mix (Applied TaKaRa, Otsu, Shiga, Japan) and performed on Applied Biosystems 7500 Sequence Detection system (Applied Biosystems, Foster City, CA, USA). The sequences of all indicated primers were listed in Table S1.

Western blotting

Cells were lysed in RIPA buffer and quantified using Bradford Protein Assay (KeyGEN BioTECH, China). Subsequently, the lysates were subjected to SDS–PAGE, transferred onto the PVDF membranes (Millipore). Then membranes were blocked with 5% BSA in PBST buffer and incubated with primary antibodies overnight at 4°C. The following primary antibodies were used: ATG14 (1:1000 dilution, ABclonal), PIK3C3 (1:1000 dilution, ABclonal), Beclin-1 (1:1000 dilution, Cell Signaling Technology), LC3B (1:1000 dilution, ABclonal), p-AKT (1:1000 dilution, Cell Signaling Technology), p-mTOR (1:1000 dilution, Cell Signaling Technology), and GAPDH (1:3000, Proteintech). Finally, the membranes were incubated with secondary antibody and developed with ECL substrate and imaged using the enhanced chemiluminescence detection system (Tennon5200, China).

Expression profile analysis of circRNAs

Total RNA of CRC tissues was extracted by using TRIzol and RNA purity was assessed by ND-1000 Nanodrop. Briefly, rRNAs were removed from Total RNA using Epicentre Ribo-Zero rRNA Removal Kit (Illumina, USA), then RNA was treated with RNase R (Epicentre, USA) and

fragmented to approximately 200bp. Subsequently, the RNA library preparation for circRNA-seq was performed by using NEBNext® Ultra™ RNA Library Prep Kit for Illumina (NEB, USA) and then sequenced on HiSeq 3000 with 2 × 150 bp mode. For circRNA-seq analysis, CIRI2 and CIRCexplorer2 were used to detect circRNAs. sequencing reads were mapped to GRCh37/ hg19 by BWA-MEM or Tophat, respectively. If a circRNA can be detected by both methods, it will be considered as an identified circRNA. Back-spliced junction reads identified in CIRI2 were combined and scaled to RPM to quantify every circRNAs.

Biotinylated miRNA pull-down assay

The capture of miR-1825-bound ceRNAs in pull-down assays with biotinylated miR-1825 was performed as described previously.[42,43] In brief, about 1×10^7 CRC cells were transfected with biotinylated miR-1825 mimics or controls (50 nM) and harvested at 48 h after transfection. The biotin-coupled RNA complex was incubated with streptavidin magnetic beads (Beaver, Suzhou, China) and then purified with Trizol for analysis.

Dual-luciferase reporter system analysis

The wild-type or mutated 3′-UTR of ATG14 gene, Beclin-1 gene or circTBC1D22A fragments were inserted into the luciferase vector. RKO cells were cotransfected with the vectors and miR-1825, which were subsequently harvested and analyzed for luciferase activity by the Luc-pair™ Duo-Luciferase HS assay kit (GeneCopoeia, China). Three independent experiments were performed.

mCherry-EGFP-LC3B fluorescence lentivirus

Autophagic flux was monitored with mCherry-EGFP-labeled LC3B lentivirus (LPP-CS-mcherry-EGFP-LC3B-Lv105-100) according to the manufacturer's introductions. LPP-CS-mcherry-EGFP-LC3B-Lv105-100 were constructed and generated by GeneCopoeia Inc. CRC cells were infected with it and the distribution of mCherry-EGFP-LC3B in cells was analyzed by confocal microscopy. After infection with mCherry-EGFP-LC3B lentivirus, in the case of autophagy, mCherry-EGFP-LC3B under fluorescence microscopy then aggregates on the autophagosomal membrane and appears as a yellow spot. The green and red dots represent phagosomes and autolysosomes, respectively, and the yellow dots represent autophagosomes. The autophagic activity is determined by quantifying the yellow dots. All experiments were repeated three times.

QUANTIFICATION AND STATISTICAL ANALYSIS

Each experiment was performed at least three times. Statistical analyses were performed using Prism 8.0 (La Jolla, CA, USA). Student's t-test and one-way analysis of variance (ANOVA) were used to evaluate the significance of the differences among different groups. The correlation analysis was detected by Pearson's correlation coefficient. All data were presented as the means ± standard deviation (SD).